Journal of Low Temperature Physics, Vol. 136, Nos. 1/2, July 2004 (© 2004)

Turnstile Behaviour of the Cooper Pair Pump

J. J. Toppari[1], J. M. Kivioja[2], J. P. Pekola[2], and M. T. Savolainen[1]

[1] *Department of Physics, NanoScience Center, University of Jyväskylä P.O. Box 35 (YFL), University of Jyväskylä, FIN-40014, Finland*
E-mail: jussi.toppari@phys.jyu.fi
[2] *Low Temperature Laboratory, P.O. Box 2200, Helsinki University of Technology, FIN-02015, Finland*

(Received December 1, 2003; revised March 15, 2004)

We have experimentally studied the behaviour of the so-called Cooper pair pump (CPP) with three Josephson junctions, in the limit of small Josephson coupling $E_J < E_C$. These experiments show that the CPP can be operated as a traditional turnstile device yielding a gate-induced current $2ef$ in the direction of the bias voltage, by applying an RF signal with frequency f to the two gates in phase, while residing at the degeneracy node of the gate plane. Accuracy of the CPP during this kind of operation was about 3% and the fundamental Landau-Zener (LZ) limit was observed to lie above 20 MHz. We have also measured the current pumped through the array by rotating around the degeneracy node in the gate plane. We show that this reproduces the turnstile-kind of behavior. To overcome the contradiction between the obtained e-periodic DC modulation and a pure 2e-behaviour in the RF measurements, we base our observations on a general principle that the system always minimises its energy. It suggests that if the excess quasiparticles in the system have a freedom to tunnel, they will organize themselves to the configuration yielding the highest current.

KEY WORDS: Cooper pair pump; Josephson tunnelling; Superconductivity; quantum bit; mesoscopic.

1. INTRODUCTION

During the last two decades lots of studies, both theoretical and experimental, have been carried out concerning the parametric pumping of charge, an idea originally introduced by Thouless in 1982.[1] This phenomenon is based on the ability of a propagating potential well to carry a charge q through a system. This again makes possible controlled

0022-2291/04/0700-0057/0 © 2004 Plenum Publishing Corporation

pumping, by periodically changing the system parameters at a frequency f to induce propagation of charge during every cycle. This yields a DC current $I = qf$ through the system.

The parametric pumping of charge can be obtained in many different kinds of devices, but most of the attention has been directed towards the systems where the charge q passed through during each cycle is quantised at a certain number of electrons, $q = -ne$, where n is an integer and the elementary charge of an electron $e = |e|$ is defined as a positive number through the paper. This can be realised, *e.g.*, by semiconductor quantum dots by varying the height of the tunnelling barriers[2] or by one-dimensional ballistic channels in a so-called SAW-pump, where the transport is induced by an acoustoelectric wave (SAW).[3,4] The most promising candidate so far is the single electron pump consisting of an array of three or more mesoscopic metallic tunnel junctions in the Coulomb blockade regime.[5–7] Due to Coulomb blockade the number of electrons in the islands of the array is very accurately controlled and the pumping can be induced by phase-shifted gate voltages,[5–7] which yield a current $I = -nef$. Here f is the frequency of the RF signal applied to the gates and the integer number n depends on the amplitude of the operating trajectory in the gate variables. These devices are more accurate than those based on semiconductors, even sufficient for metrological applications.[6,7] In the past the single electron pump has been proposed to close the metrological triangle by providing the standard for electrical current.[6–8]

The only drawback in the single electron pump is the low operating frequency $f \lesssim 5\,\mathrm{MHz}$, which cannot provide high enough current for a current standard. At higher frequencies the accuracy is lost due to coherent higher order charge transfer processes known as (in)elastic cotunnelling[9–11] and other sources of error discussed in Refs. 12–15. The maximum operating frequency could possibly be pushed higher by using a Cooper pair pump (CPP) consisting of three or more small Josephson junctions in series. The pumping in the CPP is achieved similarly by gate voltages and the charge is quantised at discrete numbers of Cooper pairs in the islands yielding a current $I = -n2ef$. Due to the different nature of Cooper pair tunnelling the operating frequency is now limited by the Landau-Zener (LZ) transitions,[16] which yields several 100 MHz for the upper limit of the frequency, depending on the parameters of the device. Due to the coherent nature of Cooper pair tunnelling, the CPP is also subject to intensive co-tunnelling, which reduces the accuracy significantly in short arrays.[17,18] To increase the accuracy one should use longer arrays or suppress the cotunnelling by other means.[19,20]

Another reason for interest in Cooper pair pumping is quantum computing, where Josephson junction circuits look promising due to their

easy scalability and relatively long decoherence times.[21–25] It has been proposed that two capacitively coupled Josephson junction arrays could form a quantum bit (qubit) and CPP could also be used to transport the information in a more complicated device.[26] When operated in suitable electromagnetic environment the CPP could also provide a method to directly measure the decoherence rate.[27,28]

In this article we concentrate on transport properties of the CPP and how the non-idealities, *e.g.*, dissipation, quasiparticle tunnelling and strong cotunnelling affect its performance.

2. COOPER PAIR PUMP

The CPP consists of three or more mesoscopic Josephson junctions in series with gate voltages capacitively coupled to each of the islands between the junctions. It is characterized by several important energy scales. The first one is the typical Josephson coupling energy E_J of Cooper pair tunnelling through the junctions and the second one is the charging energy E_C due to the small islands between the junctions. The ratio of these two, E_J/E_C, is an important parameter in determining the behaviour of the device. To be able to obtain pumping of single charges, we have to restrict ourselves to the limit $E_J \ll E_C$, where the dynamics are mainly determined by discrete tunnelling of charge carriers, i.e., Cooper pairs. In addition, the charging energy has to be larger than the thermal energy $k_B T$ to prevent thermal excitations, but smaller than the superconducting gap Δ to prevent quasiparticle poisoning.[29,30] This yields the usual chain of inequalities $k_B T < E_J \ll E_C < \Delta$.

In this article we consider a three junction CPP whose circuit schematics are shown in Fig. 1(a). Each junction has a capacitance C_k and

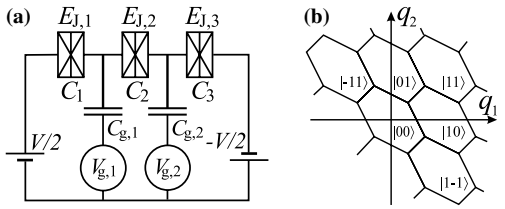

Fig. 1. (a) A superconducting array of three Josephson junctions (CPP). Here C_k and $E_{J,k}$ are the capacitance and the Josephson energy of the kth junction, respectively. (b) Stability diagram of a uniform CPP at zero bias $V = 0$ on the plane determined by the normalised gate charges $q_i = V_{g,i} C_{g,i}/2e$. The stable configuration inside each of the hexagons is shown by the kets $|n_1 n_2\rangle$.

a Josephson energy $E_{J,k}$. Gate voltages $V_{g,k}$ are assumed to be externally operated and coupled to islands with capacitances $C_{g,k}$. The Josephson phase difference φ across the array is related to the bias voltage V according to the relation $d\varphi/dt = -2eV/\hbar$.

Including only Josephson and charging energies and neglecting quasiparticle tunnelling as well as other degrees of freedom, the Hamiltonian of the system can be written as[31,17]

$$H = H_{Ch}(q_1, q_2) + H_J, \tag{1}$$

where the charging Hamiltonian $H_{Ch}(q_1, q_2)$ depends on the normalised gate charges, $q_i = V_{g,i}C_{g,i}/2e$, and the number of Cooper pairs on each island, n_i, according to $\langle n_1 n_2|H_{Ch}(q_1, q_2)|n_1' n_2'\rangle_\varphi = E_{Ch}(u_1, u_2)\delta_{n_1,n_1'}\delta_{n_2,n_2'}$, where $u_i = n_i - q_i$. This model Hamiltonian is described in detail in Refs. 18 and 32. The function $E_{Ch}(u_1, u_2)$ gives the details of the charging energy and in the presence of the bias voltage V it attains a form

$$E_{Ch} = \frac{4E_C\lambda_g}{\lambda_g^2 - 1}\left[u_1^2 + u_2^2 + \frac{2}{\lambda_g}u_1u_2 - \frac{CV}{e}\left(\frac{u_1}{\lambda_g} + u_2\right)\right] - 2peV, \tag{2}$$

where we have assumed a symmetric array with $C_1 = C_2 = C_3 \equiv C$ and $C_{g,1} = C_{g,2} \equiv C_g$. Parameter $\lambda_g = 2 + C_g/C$, $E_C = e^2/2C$ is the unit of charging energy, and p is the number of Cooper pairs tunnelled through the whole array. The Josephson (tunnelling) Hamiltonian is given by

$$H_J = -\sum_{k=1}^{3} E_{J,k}\cos(\varphi_k), \tag{3}$$

where $E_{J,k}$ and φ_k are the Josephson coupling energy and the phase difference across the kth junction, respectively.

At zero bias, $V = 0$, Eq. (2) yields a honeycomb like stability diagram shown in Fig. 1(b).[31,17] Inside each hexagon the system is stable and there is one charge state $|n_1 n_2\rangle$, i.e., the eigenstate of the charging Hamiltonian, H_{Ch}, as a ground state. At the edges of hexagons and at the triple nodes, two or three charge states are degenerate, respectively. The effect of the Josephson coupling, H_J, is to eliminate these degeneracies by introducing a coupling between different charge states. This induces new eigenstates which are superpositions of charge states and an energy gap opens between different eigenstates near the degeneracy lines of the charging part of the energy.[17,33]

Tunnelling events in CPP take place as a coherent tunnelling of Cooper pairs, in which the system travels adiabatically from the initial charge state to the final one along the eigenstate of the full Hamiltonian

of Eq. (1). This eigenstate is a superposition of the charge states with coefficients continuously varying when changing the gate charges, thus resulting in a tunnelling of a Cooper pair when a resonance in (q_1, q_2) plane is passed.[34,35] Here the resonance means that the initial and the final charge state have the same energy E_{Ch}. These resonances for coherent Cooper pair tunnelling are shown as dotted and solid lines in Fig. 2 at $V = 0$ and $V > 0$, respectively. Similar resonances for the second order process, cotunnelling of a Cooper pair, are shown by dashed lines. By co-tunnelling we mean the coherent tunnelling through two junctions simultaneously which is qualitatively similar to the co-tunnelling in normal state.[9–11] Still higher order processes are weak and play insignificant role with our sample parameters. These resonances of coherent tunnelling and cotunnelling overlap in case of $V = 0$, but separate as non-zero bias voltage V is applied. Thus, each degeneracy node is split into a triangle determined by the first order tunnelling resonances, as shown by solid lines in Fig. 2.[31,36] Inside the triangles the state of the CPP depends on the path along which the system has reached the point, thus opening the possibility for hysteretic behaviour.

Pumping of Cooper pairs at $V = 0$ is achieved by adiabatically varying the gate voltages along the path encircling one or more of the degeneracy nodes. The principle of pumping Cooper pairs is explained, *e.g.*, in Refs. 31, 17, and 18. The obtained adiabatic evolution of the eigenstates splits the transferred charge into two parts:[17,18] The pumped charge Q_{P} and the charge Q_{S} carried by the constantly flowing supercurrent I_{S}. The

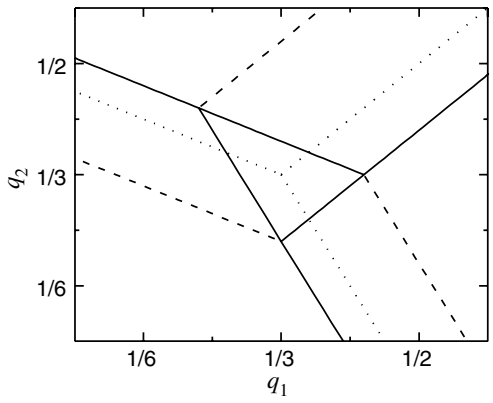

Fig. 2. Zoomed view of one of the nodes in the stability diagram of the CPP (see Fig. 1(b)). The dotted lines correspond to $V = 0$. Solid and dashed lines show the resonance condition for Cooper pair tunnelling and co-tunnelling in the presence of bias voltage $CV/2e = 0.1$.

latter one of these can be calculated as the φ-derivative of the dynamical phase $\eta_m = -\int_0^t (E_m(\tau)/\hbar)\, d\tau$ in the state $|m\rangle$, $Q_S/2e = -\partial\eta_m/\partial\varphi$, while the pumped charge is related to the φ-derivative of Berry's phase[37] $\gamma_m = i \oint \langle m|dm\rangle$ attained along the pumping path, $Q_P/2e = -\partial\gamma_m/\partial\varphi$.[38]

3. SAMPLE FABRICATION

The sample used in experiments was fabricated by e-beam lithography with a conventional self-aligning shadow angle evaporation technique. The two different *ex situ* process steps were performed to make it possible to first evaporate large scale structures containing all the contact pads for bias and gate lines and the large guard planes isolating these various entries. These guard planes were permanently grounded by bonding them to the bottom of the sample holder. The undesirable capacitive crosscouplings between the lines were eliminated this way effectively as will be seen later. The design of the large scale structures is shown in Fig. 3(a). These large structures were fabricated of gold to ensure good electrical contact in ultrasonic bonding of wires on the sample stage, and between the two layers fabricated *ex situ*. The so-called quasiparticle traps in biasing lines near the sample were also evaporated at the same time.[39,30] These quasiparticle traps consisting of a $2.5\ \mu\text{m} \times 0.6\,\mu\text{m} \times 60\,\text{nm}$ sheet of gold were placed under the biasing line about $4\,\mu$m away from the outermost junctions.

The sample itself is surrounded by these large scale structures and it consists of three Josephson junctions of about $100\,\text{nm} \times 100\,\text{nm}$ in area. The two $\sim 1\,\mu$m long islands had an interdigital type of design to improve the gate coupling and to suppress the crosscouplings. The gate lines were also brought to the sample via a $1.8\,\mu$m wide channel between the guard planes. The small structures were fabricated out of aluminium with aluminium oxide as a barrier in the tunnel junctions.

4. CHARACTERISATION OF THE SAMPLE

4.1. Experimental Setup

The experimental setup is shown in Fig. 4(a). All measurements were done in an S.H.E. Corporation DRI-420 dilution refrigerator whose minimum temperature is $\sim 10\,\text{mK}$. Lower parts of the cryostat are surrounded by lead over the vacuum jacket in the helium bath for magnetic shielding.

The fridge has 14 highly filtered lines for DC signals (Fig. 4 (a)). These lines include 3-stage low pass filtering at different temperatures. At room temperature we used commercial low pass π-filters (Tusonix 4101,

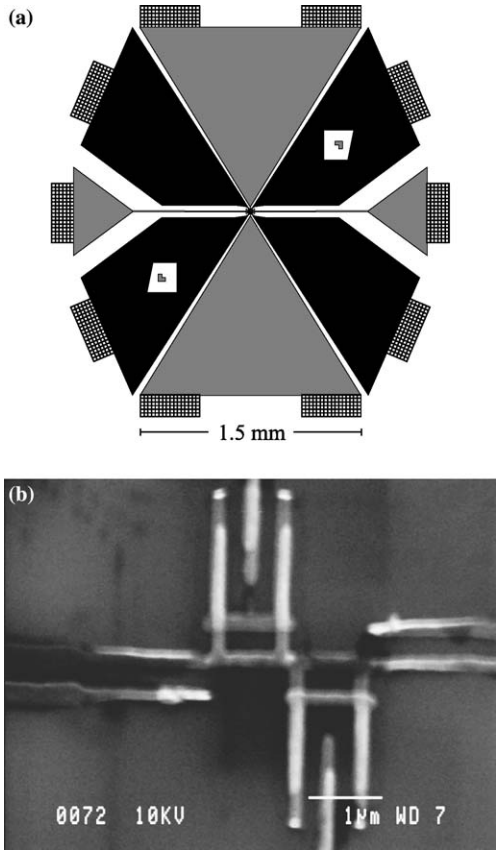

Fig. 3. (a) Scheme of the large scale structures of the sample. Gray areas at the sides indicate biasing lines and the triangular ones gate lines at the top and the bottom. Black areas show the large guard planes to suppress parasitic crosscouplings. Grid-like areas in the contact pads are used in ultrasonic bonding, and they improve the mechanical strength of the contact. Also the two bigger alignment marks are seen inside the two guard planes. (b) An SEM-image of the small structures of the sample used in these experiments. The interdigital type design of the gates lowers the crosscoupling between them. The large guard planes as well as quasiparticle traps fall outside the image.

-55 dB at 100 MHz) which were connected directly to the top of the cryostat. From room temperature down to 600 mK all DC signals are fed through coaxial cables with Nb as an inner conductor and stainless steel as shielding. Between 600 and 60 mK plate each line has 1.5 m of Thermocoax® cable which also forms the next filtering stage (-200 dB at 20 GHz).[40] At both ends of Thermocoax® cables there are 1 kΩ resistors

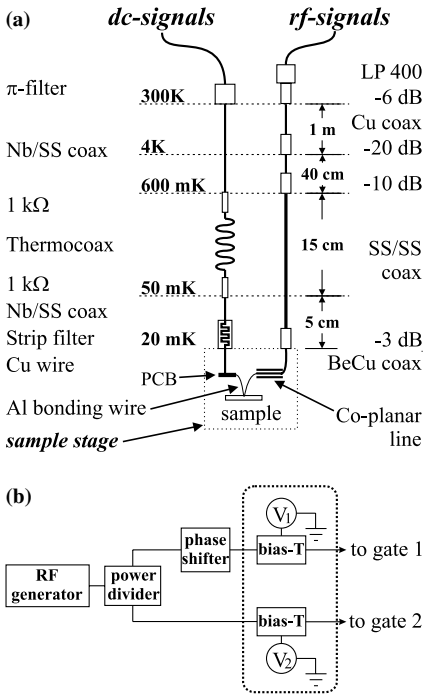

Fig. 4. (a) Measurement wiring of the dilution refrigerator. (b) A schematic picture of the room temperature RF signal connections. The dotted line shows the part included in the integrated domestic circuit. The compensation circuit was not needed in the measurements due to low crosscoupling in the sample.

in series to improve filtering at low frequencies (< 1 GHz). The last filtering stage is at the sample stage at the base temperature. These filters were commercial stress gages (KYOWA KFG-2-350-D1-23) squeezed between two ground planes forming continuous RC strip line filters.[41] Short sample stage wires were made of Cu and were soldered to a printed circuit board (PCB). This again was ultrasonically bonded to the DC electrode of the sample with aluminum wires.

Our refrigerator has four lines for RF signals (Fig. 4 (a)). At room temperature we used 400 MHz low pass filters (Mini-circuits SBLP-400) and -6 dB fixed attenuators (Inmet). These were directly connected to the top of the cryostat and all other room temperature connections were made by using flexible SUHNER Sucoflex 104P cables with SMA connectors. From room temperature down to 4 K RF signals are fed through Cu coaxial cables. At low temperatures we use BeCu coaxial cables, except

between 600 mK and the sample stage we use semirigid stainless steel coaxial cables for better thermal isolation. As a whole the RF lines have -33 dB attenuation at low temperatures: -20 dB at 4 K, -10 dB at 600 mK and -3 dB at sample stage temperature (Inmet fixed attenuators). At the sample stage we use MCX connectors and all other connectors are of SMA type. The sample is directly ultrasonically bonded by Al bonding wire to a coplanar transmission line mounted on the sample stage. When all these lines are connected to the coldest parts of the refrigerator, the base temperature is lifted up to ~ 20 mK, as compared to the ~ 10 mK base temperature without RF lines.

All DC voltage measurements were done by using HMS Electronics model 568 low-noise preamlifiers and for current measurements we used DL-Instruments 1211 preamplifier. Both amplifiers were powered by battery sources only. Between preamplifier and data acquisition (NI PCI-6036E DAQ card) we use a home made battery powered analog opto-isolation to avoid ground loops and digital noise in our measurements. In Fig. 4(b) we show a schematic picture of gating signal connections. For this we used a HP8656B signal generator and divided the RF signal by using an INMET 6014-2 power divider. One of these signals was fed through a phase shifter while the other went directly into the home made circuit schematically consisting of two bias-Ts and a possibility to add negative crosscoupling between the two signals to compensate the undesirable capacitive coupling between the gates in the CPP. The circuit also contained a high quality RF circuit board and optoisolated linking to the computer which could be used to program all the gains used in bias-Ts, DC offsets, compensation and as a main amplification. The control program also included possibility to automate the measurements to some extent.[42]

4.2. Current-Voltage Dependence

In Fig. 5 we present I–V characteristics of the sample, taken with different combinations of gate voltages $V_{g,1}$ and $V_{g,2}$. It shows a sharp rise at the beginning of the quasiparticle tunnelling branches at bias voltages $V \simeq \pm 6\Delta_{Al}/e \approx \pm 1.2$ mV. Also all four major peaks in subgap regime corresponding to different possibilities of Josephson-quasiparticle (JQP) cycles are clearly visible.[35,43–45] The gate modulation is most pronounced at the gap edge as well as in the region of JQP-peaks. From the asymptotic slope of the I–V curve at high voltages we obtain the normal state resistance per junction, $R_T \simeq 34\,\mathrm{k}\Omega$, which yields $E_J = \Delta_{Al} R_Q / 2R_T \approx 19\,\mu$eV. Here we have assumed that all junctions are identical and that the critical current obeys the Ambegaokar-Baratoff relation.[46,47] $R_Q = h/(2e)^2$

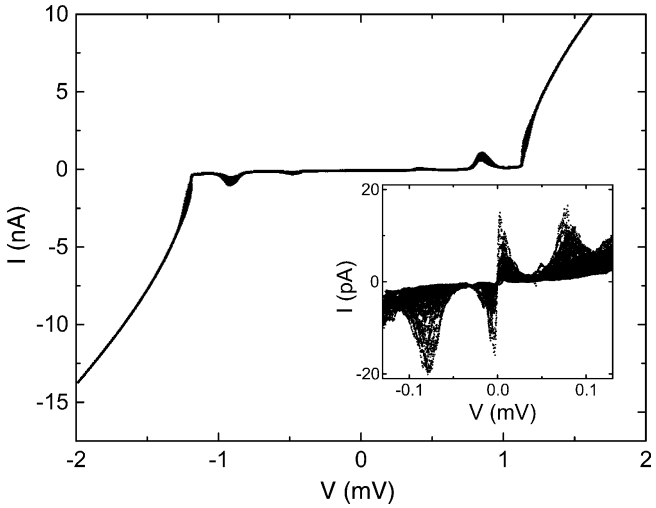

Fig. 5. *I–V* characteristics of the measured sample, taken at different combinations of gate voltages $V_{g,1}$ and $V_{g,2}$. The inset presents the blow up of the *I–V* curves near zero bias.

is the resistance quantum for Cooper pairs. The value of the charging energy, $E_C \approx 129\,\mu$eV, was obtained using the depth of the dip in the normal state conductance curve taken at 4.2 K.[48] This yields $E_J/E_C \approx 0.15$. Since the charging energy is well below the superconducting gap $E_C < \Delta_{Al} \approx 200\,\mu$eV, the parity effect should not be suppressed.[34,49]

The capacitances of the tunnel junctions, $C_T \approx 0.62$ fF, can be calculated using the E_C measured as described above, while the gate capacitances, $C_{g,i} \approx 70$ aF $(i = 1, 2)$, were obtained from the periodicity of the current modulation at high bias. There exists also unavoidable cross-couplings, i.e., capacitive coupling of the gate voltage $V_{g,1}$ to the second island, C_{12}, and vice verse, C_{21}. These parasitic capacitances can be estimated from the slope of any known horizontal or vertical periodic structure in the modulation plane similar to the one in Fig. 6, where the current is plotted as a function of the two gate voltages $V_{g,i}$. We found crosscoupling to be $C_{12} \approx C_{21} \sim 0.16 C_g$, which is evidently low enough for independent operation of the two gates.

We did not apply any active compensation to cancel out the effect of the crosscoupling, since during the turnstile like *in-phase measurement*, explained later in Section 5, the gates were operated simultaneously and due to that the only effect of the crosscoupling was to slightly increase the amplitude of the chosen path, which has been taken into account when calculating the real amplitudes. In the pumping measurement, later called

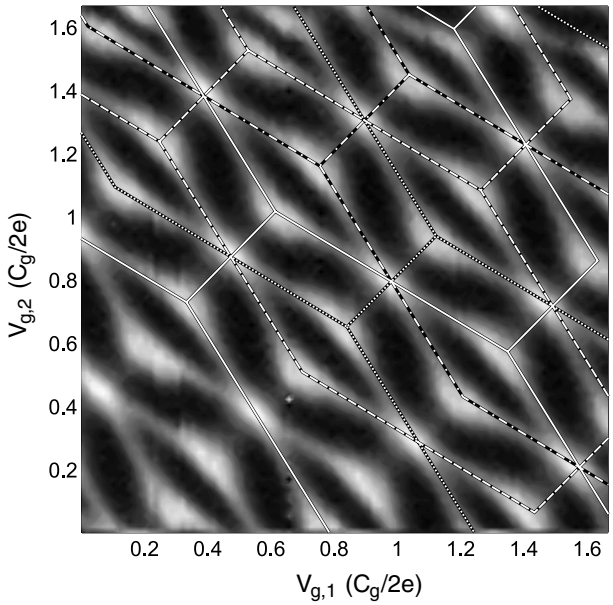

Fig. 6. Supercurrent I_S as a function of two gate voltages $V_{g,1}$ and $V_{g,2}$. The lighter the color is, the higher is the current. The structure is composed of four different $2e$-periodic honeycombs each corresponding to the expected stability diagram of the CPP. These honeycombs are separated by half a period due to different configuration of quasiparticles, which act like discrete variations in the gate charges. Lines drawn in the figure present each one of these different honeycombs in the case of a uniform array, i.e., an array with $C_1 = C_2 = C_3$, and they fit the data exactly, with the gate capacitances $C_{g,i}$ and the crosscouplings, C_{12} and C_{21}, as fitting parameters. A small bias voltage of $V \sim 15\,\mu$V was applied during the measurement to sit approximately at the maximum of the supercurrent.

as *out-of-phase measurement*, the crosscoupling would have an effect on the amplitude of the pumped current if we were operating at coherent regime.[17,18,32] Yet, according to our estimation for the decoherence time in our measuring setup we are operating solely incoherently and small variations in the pumping path should not significantly affect the result. However, we also tried to apply an active compensation but since no significant change in results that would alter any conclusions was observed, we turned the active compensation circuit off for simplicity.

In the large scale figure the current around zero bias is not visible but it is seen in the blow up. The supercurrent, i.e., the feature around zero bias, depends strongly on the gate voltage. It is peaked around $V = 0$, getting the maximum at $|V| \ll E_C/e$ (see Fig. 5). The shape of supercurrent also indicates the presence of the electromagnetic environment $Z(\omega)$

with low impedance of $0 < \mathrm{Re}[Z(\omega)] \ll R_\mathrm{Q}$.[50] This agrees well with the impedance of the biasing lines, $\mathrm{Re}[Z(\omega)] \sim \sqrt{\ell/c}$, which is of the order of the vacuum impedance $377\,\Omega$. Here ℓ and c are the inductance and the capacitance per unit length, respectively, and the resistance of the normal metal sections, $R \sim 1\,\Omega$, is negligible. Resonance peaks symmetrically around zero bias at $V \approx \pm 80\,\mu\mathrm{V}$, are also visible in this figure, and they will be discussed later.

4.3. Gate Modulation

To find the correct working point for pumping we mapped out the gate dependence of the supercurrent $I_\mathrm{S}(V_{\mathrm{g},1}, V_{\mathrm{g},2})$ by applying a small bias voltage to maximize I_S and measuring the current while passing systematically all combinations of gate voltages. Since $I_\mathrm{S} = -(2e/\hbar)(\partial H/\partial\varphi)$ it is clear that it should follow the honeycomb like stability diagram of the CPP (see Fig. 1(b)), getting an increase at every degeneracy line and maximum value at the triply degenerate nodes. The modulation curve obtained experimentally is presented as a contour plot in Fig. 6. It does not show the expected pure honeycomb-like structure, which indicates the existence of non-equilibrium quasiparticles in our system. Yet, the pattern cannot be ascribed to pure quasiparticle tunnelling either. We have observed this kind of a modulation pattern in most of the (more than 10) measured samples.

The effect of quasiparticles tunnelling into and out from the islands is to change the gate charge by one electron and thus to shift the $2e$-periodic stability diagram half a period (i.e., e-period) in the corresponding direction. If the rate of these tunnellings is higher than inverse of the measuring time, $\tau_m \geq 100\,\mu\mathrm{s}$, the current obtained is an average over many $2e$-periodic honeycombs separated by half a period in the direction of one of the two gate charges. Since the shift due to quasiparticle tunnelling is exactly half the period of the stability diagram, two shifts in same direction restores the original honeycomb pattern. This feature can be seen in the charging Hamiltonian, H_Ch, i.e., tunnelling of two quasiparticles through the same junction has the same effect on the charging energy as a tunnelling of a Cooper pair. Thus, any quasiparticle configuration $(n_{\mathrm{qp},1}, n_{\mathrm{qp},2})$ can be reduced to $\{\tilde{n}_{\mathrm{qp},i} = n_{\mathrm{qp},i} \mod 2\}_{i=1,2}$ and it is enough to consider only four different honeycombs corresponding to, *e.g.*, quasiparticle distributions $(0,0)$, $(1,0)$, $(0,1)$ and $(1,1)$.

As expected, the measured pattern of Fig. 6 is composed of four shifted $2e$-periodic honeycombs each corresponding to the stability diagram of the CPP in the absence of quasiparticles. These four honeycombs each displaced by half of the $2e$-period are illustrated as lines. The lines

are fitted to the data with the gate capacitances and crosscouplings as fitting parameters and they correspond to the symmetric array. In addition to the regular degeneracy nodes the pattern shows some extra peaks which can be explained as intersections of different honeycombs. In these points the supercurrent is high in three out of four different quasiparticle configurations, yielding a resonance peak.

In the preceding paragraphs the measured modulation pattern consisting of four shifted honeycombs was explained by quasiparticle tunnelling, which was assumed to happen fully stochastically in both time and direction. This is the usual assumption in mesoscopic superconducting devices consisting of Josephson junctions.[51] However, we can also explain these four honeycombs by means of quasiparticle tunnelling and by assuming that *the system with degrees of freedom evolves via states of the lowest energy.* In case of a biased array, the system can always lower its energy by increasing the number p of Cooper pairs tunnelled through it. Thus, it will try to maximize the current. If we consider the system as a whole including quasiparticles and assume them to have a freedom to tunnel, they will organize themselves to the configuration yielding the highest current. Thus, the quasiparticle tunnelling events are still happening stochastically in time but not in direction. This possibility of quasiparticles to tunnel can be clearly observed in Fig. 6 and it can be justified by the same means as in the fully stochastic model.[51]

According to *energy-minimisation* the system always changes the quasiparticle configuration to the one corresponding to maximum supercurrent, while varying the voltages $V_{g,i}$ in the measurement of the gate modulation. Thus, this model yields the same combination of four honeycombs for the measured current, as we would obtain if the quasiparticle configurations changed fully stochastically. However, in our model the current is higher because it is not the time average over many configurations but the largest possible. Unfortunately, by measuring the gate modulation it is impossible to distinguish between the fully stochastic and the energy-minimisation models and find out which one is the valid explanation. Later we argue for the latter explanation based on the results of the RF measurements.

However, neither of the previous models for quasiparticle tunnelling explain why sometimes the $2e$-periodicity is seen and sometimes not, even though the sample parameters should yield the clear parity effect. To further examine this, we can make a 'worst case' assumption that quasiparticles always have freedom to move (due to, *e.g.*, extra subgap quasiparticle states in the samples). Then the quasiparticle tunnelling rate Γ would be essentially determined by the charging energy and the general golden rule expression (in the limit $E_C \gg k_B T$): $\Gamma \approx$

$E_C/(e^2 R_T^*)\exp(-E_C/k_B T)$, where $R_T^* = R_T/\eta^2$ and $\eta \simeq 10^{-4}$ is the relative density of quasiparticle states inside the gap.[52,53] According to our sample parameters and with temperature of 30 mK, this yields $\sim 10^{55}$ h for the average time between the quasiparticle tunnelling events, which is infinite in the time scale of the measurements. Yet, this time depends strongly on the temperature and if the electronic temperature of the sample would be higher, *e.g.*, 300 mK, which could be the case due to inadequate filtering or thermalisation of the measurement lines, the time between the quasiparticle tunnelling events would be ~ 500 ms resulting in e-periodicity in the measurement. This argument yields the same threshold temperature of $\sim$250 mK for $2e$-periodicity as the earlier measurements in Refs. 48, 39, and 30, and could explain the lack of the $2e$-periodicity in some cases.

4.4. Effect of the Bias Voltage

Applying bias voltage V changes the stability diagram so that each degeneracy node is split into a triangle as discussed in Section 2. These triangles are clearly visible at the modulation plane measured at $V \simeq 64\,\mu$V and shown in Fig. 7(b). Also theoretically calculated degeneracy lines giving a resonance condition for Cooper pair tunnelling are drawn in the figure. These lines are calculated using the parameters obtained earlier for the measured sample. Fig. 7(a) shows the same modulation plane but at $V \simeq 0$. The triangles are formed around the nodes of each honeycomb in Figs. 7(a) and 6, and the 'extra' nodes formed of intersections of different honeycombs disappear as they should.

With a more detailed inspection one finds the measured current to be slightly increased also at resonance lines for co-tunnelling, which is not seen at the (current) scale of Fig. 7(b). Good agreement between theoretical resonance lines and experimental data and also the reduction of the current inside the triangles proves the measured current to be mainly carried by the supercurrent, I_S. Thus, quasiparticles present in the system are not acting as major carriers of current, which can be the case due to Coulomb blockade and the energy gap Δ. The inelastic tunnelling of Cooper pairs, where energy is interchanged between the tunnelling Cooper pair and other parts of the system, *e.g.*, electromagnetic environment or quasiparticles, is also not important.[50] Both these phenomena should increase current inside the whole triangle.[36]

The first resonance peaks in the I–V curve at $V \simeq 80\,\mu$V (see inset in Fig. 5) can also be explained by the effect of the bias on the stability diagram. At $V \simeq 0$ we have the highest current flowing at the triple nodes and at the 'extra' nodes, which are also three times degenerate. After increasing V the nodes are split and the maximum current appears at the doubly

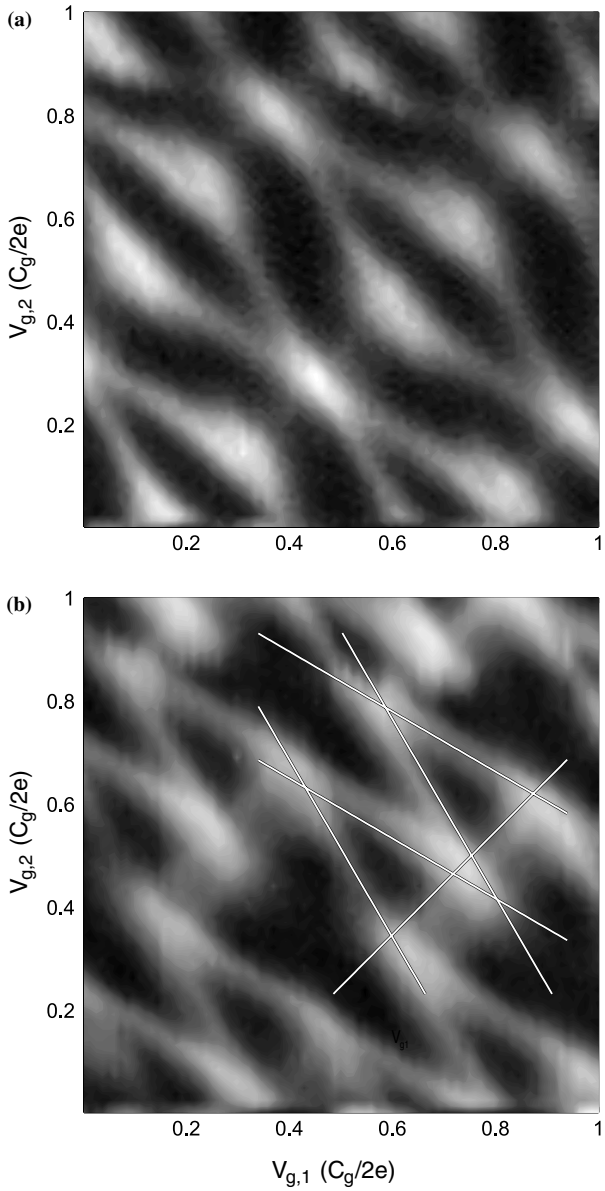

Fig. 7. Supercurrent I_S as a function of two gate voltages $V_{g,1}$ and $V_{g,2}$ with two different bias voltages applied: (a) $V \simeq 0$ (adjusted to the maximum of the supercurrent) and (b) $V \simeq 64\,\mu$V. The lighter the color is, the higher is the current. In (b) the theoretically calculated resonance conditions for coherent tunnelling of Cooper pairs is presented as lines. These lines coincide with the pattern of enhanced current in the experimental data.

degenerate sites, yielding much lower current than at triple nodes of $V \sim 0$. The new triply degenerate nodes are formed when the triangles situated close to each other overlap upon increasing V and the maximum of the current is reached when vertices of the neighbouring triangles coincide, as is approximately the case in Fig. 7(b). The closest nodes correspond to different quasiparticle configurations, $(0, 0)$ and $(1, 1)$ and are situated along the lines $V_{g,2} = V_{g,1} + k/2$, where k is an integer number, as seen in Figs. 6 and 7(a). Using parameters obtained for this sample we estimate the new triple node to be formed between neighbouring zero bias nodes at $V = 83\,\mu$V, which is exactly the voltage where the highest resonance peaks are located in the experimental I–V curve.

5. OPERATION AS A TURNSTILE

5.1. Principle of Operation

A conventional turnstile for electrons or Cooper pairs consists of two arrays ($N \geq 2$) of junctions connected by a common island in between, whose charging and discharging can be controlled by a gate.[54,55] The charging sequence is additionally controlled by the applied bias voltage, which determines the direction of the obtained DC current when an AC voltage is applied to the gate at frequency f. Each gate voltage cycle charges and discharges the island unidirectionally, thus generating a current $I = -ef$.

The CPP can operate as a turnstile because of the hysteretic behaviour within a finite bias triangle, opened around node in the modulation plane. The simplest way to describe this behaviour is to consider a path in (q_1, q_2) plane with the constraint $q_1 = q_2$, exiting the triangle at both extremes (see Fig. 8(a)), and to assume that at every resonance, i.e., at each degeneracy of the charging Hamiltonian, H_{Ch}, the system is driven to the state with lower energy. This simple reasoning alone is enough to explain the turnstile kind of behaviour: within every traversal of the path one Cooper pair is transferred through the array in the direction of the bias voltage. This principle of operation involves coherent tunnelling, cotunnelling and relaxation. It is shown in Fig. 8 and explained in more detail later.

To obtain this hysteretic behaviour one needs dissipation in the system. This can be provided, *e.g.*, by the electromagnetic environment or quasiparticles, which both can absorb any amount of energy dissipated in the system. Without dissipation the adiabatic passing through the degeneracy line of charging energy H_{Ch} will retain the eigenstate of the system, i.e., the gap of E_J is not crossed. This will induce coherent tunnelling of

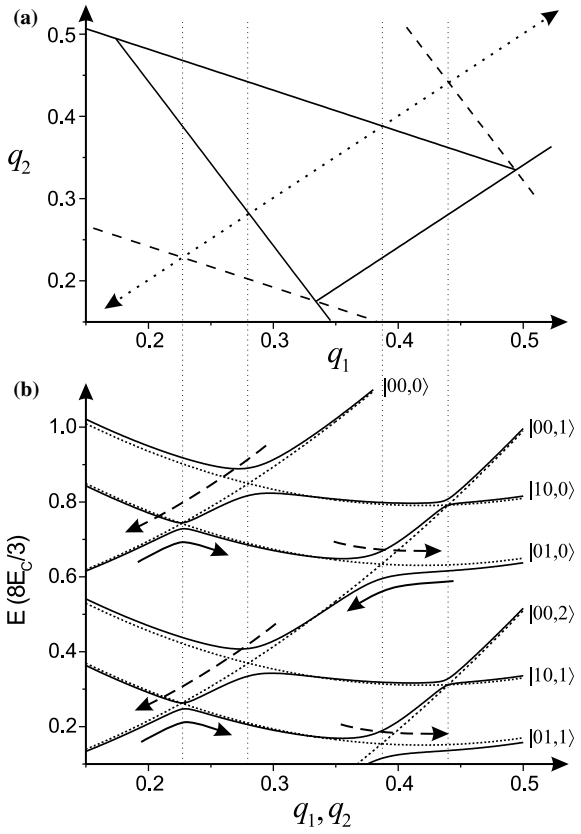

Fig. 8. (a) The path $[t \mapsto (q_1, q_2) : q_1(t) = q_2(t)]$, used in the turnstile measurements (dotted line). It is centered at the degeneracy node of $V = 0$ and exits the triangle around this node at both extremes. (b) Energy diagram of the CPP plotted along the path in (a). The solid lines represent the eigenstates of the system and the dashed lines are energies of the pure charge states of H_{Ch}, which are indicated at right by kets. The arrows show the method of transferring one Cooper pair per cycle through the CPP in the direction of the bias voltage as in a turnstile. The dashed arrows correspond to the relaxation into the lower energy eigenstate at around resonances while the solid arrays indicate coherent tunnelling or co-tunnelling. The thin vertical dotted lines are there to clarify corresponding locations between (a) and (b). The diagram has been calculated using parameters $E_{\mathrm{J}}/E_{\mathrm{C}} = 0.2$ and $CV/2e = 0.16$.

one Cooper pair in the direction which depends whether the system is in the ground or in the excited state. The limit for the adiabaticity is determined by the probability of band crossing, the so-called LZ tunnelling.[16] This probability can be written as[33,56]

$$P_{\mathrm{LZ}} = \exp\left(-\frac{\pi E_{\mathrm{J}}^2}{8\hbar E_{\mathrm{C}}\dot{q}}\right) \equiv \exp\left(-f_{\mathrm{LZ}}/f\right), \tag{4}$$

where $q = \sqrt{q_1^2 + q_2^2}$ is the absolute length in the (q_1, q_2) plane. In the absence of dissipation the probability for band crossing is equal in both directions, i.e., to excite or relax the system, but with dissipation the symmetry breaks. The probability to excite the system retains the same amplitude, P_{LZ}, but the probability for relaxation $P_{\mathrm{Rel}} = 1 - P_{\mathrm{LZ}} + P_{\mathrm{LZ}}^2$ is significantly increased and reaches almost unity in the case of strong coupling to a dissipative element.[33,56]

How this effect of dissipation makes it possible to use CPP as a turnstile is explained in Fig. 8(b), where the energy diagram of the CPP is plotted along the path with time t as a parameter $[t \mapsto (q_1, q_2) : q_1(t) = q_2(t)]$ crossing the triangle as shown in Fig. 8(a). To be able to properly explain the behaviour we have to include the number of Cooper pairs tunnelled through the array to our notation: so, instead of $|n_1 n_2\rangle$ we write $|n_1 n_2, p\rangle$.

If the system is initially at the state $|00, 0\rangle$ and we start to increase both gates, i.e., moving from left to right along the x-axis in Fig. 8(b), we come to the point of resonance for tunnelling through two junctions simultaneously, i.e., cotunnelling, to the state $|01, 0\rangle$. This resonance condition is indicated by a dashed line in Fig. 8(a). In the case of cotunnelling the total coupling for one Cooper pair to tunnel through two junctions, $E_{\mathrm{J}}^{\mathrm{co}}$, depends on the E_{J} of the junctions and the energy of the intermediate virtual state. Using the second order perturbation theory and the value $V = 50\,\mu\mathrm{V}$ used in measurements (see Section 5.2) we obtain $E_{\mathrm{J}}^{\mathrm{co}}/E_{\mathrm{J}} \approx 0.28$ yielding the LZ frequency $f_{\mathrm{LZ}}(E_{\mathrm{J}}^{\mathrm{co}}) \approx 65\,\mathrm{MHz}$. This indicates the adiabatic condition to hold during gate excursion and cotunnelling to happen with frequencies smaller than 65 MHz. When continuing along the path, the system is retained in state $|01, 0\rangle$ due to relaxation at resonance crossed. When coming back along the same path the system is driven to the state $|00, 1\rangle$ due to a first order resonance, shown by a solid line in Fig. 8(a), yielding coherent tunnelling and the system is kept there by relaxation (see Fig. 8(b)). Then the cycle starts over again with $|00, 1\rangle$ as an initial state. Since the situation is fully asymmetric with respect to bias, the operation carries one Cooper pair per cycle through the array in the direction of the applied bias voltage V.

The most significant source of errors in the cycle described above is the inelastic tunnelling of a Cooper pair, which is also induced by the dissipation and is proportional to the function $P(E)$,[50] which gives the probability density of a tunnelling Cooper pair to emit (absorb) energy E $(-E)$

to the electromagnetic environment. In addition, the presence of quasiparticles increases this probability by providing another way to exchange energy. Examples of possible undesirable inelastic tunnelling events are shown in Fig. 9 by wavy arrows numbered as 1. As one can figure out from the energy diagram, these are not affecting the outcome of the gate cycle unless several of them occur during one cycle. This would induce transfer of two or more Cooper pairs during that particular cycle as in the example shown by thick solid arrows in Fig. 9. Also similar inelastic relaxation events which would instantly destroy the outcome of the excursion, are indicated. Fortunately though, these relaxation processes are likely to be largely suppressed due to the large number of virtual tunnelling events, i.e., higher order of cotunnelling, needed in them. These processes are shown by thin wavy arrows striked out and numbered as 2. Thus, the system is fairly rigidly 'locked' to transfer only one Cooper pair per cycle.

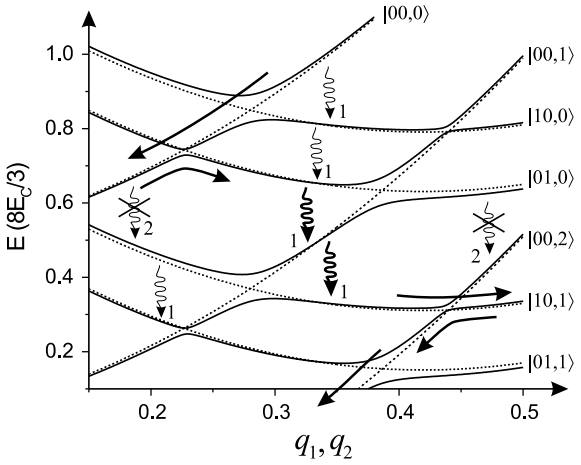

Fig. 9. Evolution of the CPP along the gate path of Fig. 8(a). The wavy arrows numbered as 1 show a couple of examples of possible undesirable inelastic tunnellings of a Cooper pair (or of two quasiparticles), which is the most significant source of errors in the cycle of Fig. 8(b). However, these are not affecting the final outcome of the gate cycle unless there happens several of them during one cycle. The thick solid (straight and wavy) arrows show an example of a cycle with several inelastic tunnelling events. The charge transferred in that particular cycle is two Cooper pairs, i.e., $4e$. Striked out arrows numbered as 2 indicate similar inelastic relaxations which would instantly induce errors in pumping. These are fortunately suppressed due to the large number of intermediate tunnelling events needed.

5.2. Measurements

To test whether the former line of reasoning holds we first measured the gate dependence of the current at a small bias voltage, $0 < V < 80\,\mu$V, and 10 MHz sinusoidal signals added on top of the DC voltages $V_{g,i}$ applied to both gates. The AC signal was fed to both gates at the same phase and the amplitude was 1/6 times the $2e$-period, thus corresponding to the path drawn in Fig. 8(a). The obtained current as a function of DC gate voltages is plotted in Fig. 10. The white dotted lines show the structure measured without the RF signals at $V \simeq 0$. Data clearly indicate the enhancement of current inside the areas of the triangles as predicted in the previous chapter.

To obtain more quantitative results we froze the DC gate voltages to the values corresponding to one of the degeneracy nodes and applied a similar sinusoidal signal as before at different frequencies. The full I–V dependence was measured instead of sitting at a fixed bias voltage to better find the correct bias voltage, $0 < V < 83\,\mu$V, where the applied gate path

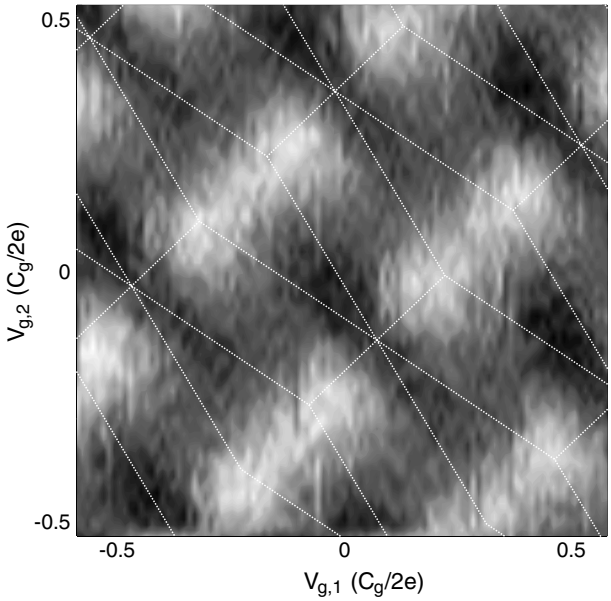

Fig. 10. Current with small bias voltage, $0 < V < 80\,\mu$V, as a function of two DC voltages applied to gates $V_{g,1}$ and $V_{g,2}$ with 10 MHz in-phase sinusoidal signals added to the two gates. The amplitude of the sine was $1/6 \times 2e$-period. The measured structure of the modulation without RF signals and at $V \simeq 0$ is drawn as white lines.

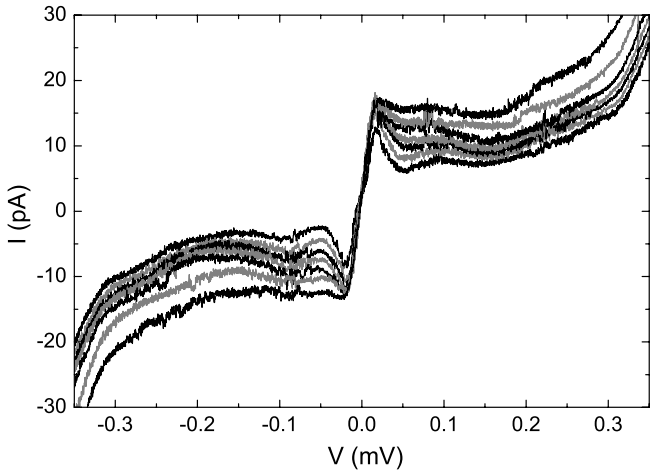

Fig. 11. The I–V curves measured with DC gate voltages tuned to one of the degeneracy nodes and in-phase sinusoidal RF signals added to the two gates. Amplitude used was $1/6 \times 2e$-period and frequencies corresponding to I–V curves from lowest to highest absolute current level are 0.5, 6, 12, 18, 26, 40, and 60 MHz.

would be optimum for turnstile kind of behaviour. Some of these measured I–V curves are shown in Fig. 11.

From the I–V curves we can recognize the resonance point at $V \simeq 80\,\mu\mathrm{V}$ and the optimum operation point is the minimum between that and zero voltage, i.e., around $V \simeq \pm 50\,\mu\mathrm{V}$. If we extract the current at $V = 50\,\mu\mathrm{V}$ and plot it against f we obtain the dependence shown in Fig. 12. The dashed line of the inset shows the ideal $I = -2ef$ dependence which should be obtained if the device operates as a turnstile as explained in the preceding section.

At low f ($\leq 10\,\mathrm{MHz}$) the current increases as $I \simeq -2ef$ but starts to lag behind at around 25 MHz. To find out whether this behaviour is consistent with LZ crossing, we fitted the data using

$$I = -2ef\,[1 - P_{\mathrm{LZ}}(f)] + I_0. \tag{5}$$

The fitting parameters used were the starting slope ($\sim 2e$), LZ frequency f_{LZ}, and the *static leakage current* I_0, which is the current flowing at the present operating point, i.e., at given value of V and DC values of $V_{\mathrm{g},1}$ and $V_{\mathrm{g},2}$, but without any AC excitation applied to the gates. This formula did not fit properly the data, mostly due to the non-zero asymptotic slope of our data at high frequencies. To take this extra slope into account we modified the fitting function to allow for a finite leakage current with

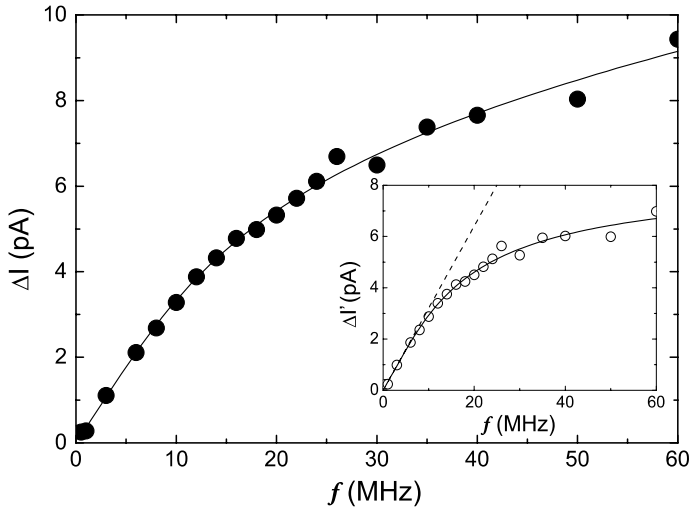

Fig. 12. Current in a cycle through the degeneracy node (see Fig. 8(a)) as a function of the frequency of the RF signals applied in-phase to the two gates. For clarity the static leakage current I_0 (see Eq. (6)) has been subtracted, i.e., $\Delta I = |I - I_0|$. The bias voltage was $V \simeq 50$ μV and the AC amplitude was $1/6 \times 2e$-period. The solid line is the fit by Eq. (6) and values for the fit parameters are shown in the first line of Table I with the exception of I_0. The inset shows the same current with the dynamic leakage current also subtracted, i.e., $\Delta I' = |I - I_0 + 2ef\,Q_L|$, and the dashed line shows the ideal $2ef$ dependence predicted by the theory.

linear dependence on f. The function which we used to fit the data and which is shown in Fig. 12, is of the form

$$I = -2ef\,Q_P[1 - \exp(-f_{LZ}/f)] - 2ef\,Q_L + I_0, \tag{6}$$

where the fit parameters are f_{LZ}, I_0, Q_P and Q_L. Here Q_P and Q_L are the charges transferred and leaked during one cycle in units of $2e$, respectively.

The existence of this frequency dependent *dynamic leakage current*, $-2ef\,Q_L$, during the AC gate operation, can be physically justified as the result of undesirable inelastic tunnelling of Cooper pairs. As explained earlier, these inelastic tunnelling events can happen inside the triangle during the operation and their contribution to the resulting current is, due to the fact that at the minimum two tunnelling events per cycle are needed to affect the outcome, small but non-zero. If we assume the probability for inelastic tunneling P_{IT} to be independent of frequency, we obtain an approximate expression for the static leakage current, $I_{leak} = -[2eP_{IT}^2 + \mathcal{O}(P_{IT}^4)]f$, which depends linearly on f. The total current is thus of the form $I = -2ef[1 - P_{LZ}(f)] + I_{leak}$ and $Q_L \sim P_{IT}^2$ in Eq. (6).

TABLE I

Fit parameters using Eq. (6) under various experimental conditions. The current scale was shifted to set I_0 to zero

Ampl. (2e)	Bias	Q_P (2e)	f_{LZ} (MHz)	Q_L (2e)
1/6	$V>0$	0.985 ± 0.068	26.2 ± 4.4	0.127 ± 0.046
1/6	$V<0$	0.956 ± 0.080	29.1 ± 6.5	0.142 ± 0.068
1/4	$V>0$	0.996 ± 0.049	35.1 ± 4.4	0.132 ± 0.031
1/4	$V<0$	0.976 ± 0.100	24.7 ± 5.0	0.229 ± 0.030
1/3	$V>0$	4.0 ± 2.3	3.5 ± 1.8	0.546 ± 0.029
1/3	$V<0$	3.8 ± 1.3	4.4 ± 1.4	0.481 ± 0.027

Equation (6) fits perfectly the data and the values of the fit parameters obtained using it are shown in Table I. The analysis of the data was done both at negative and positive bias voltages. As explained earlier, the obtained current changes sign with bias voltage. We also repeated the measurement in another node with slightly larger amplitude ($1/4\times 2e$-period) of RF signal and these results are also shown in Table I.

As seen in Table I, the obtained frequency dependence agrees with the theoretical prediction of $-2ef$ at low frequencies, i.e., $Q_P\simeq 1$. However, the LZ frequency obtained, $f_{LZ}\sim 30\,\mathrm{MHz}$, is lower than that estimated ($\sim 50\,\mathrm{MHz}$) for cotunnelling. This discrepancy can originate from the inhomogeneity of the sample. Since P_{LZ} is an exponential function of E_J, it is the smallest $E_{J,i}$ in the array that determines the LZ threshold. The value $f_{LZ}\sim 30$ MHz yields $E_J\approx 17\,\mu\mathrm{eV}$ which is a very reasonable value since the corresponding number estimated for a symmetric array is $19\,\mu\mathrm{eV}$. For the leaked charge we obtained $Q_L\sim 0.17$, which corresponds to a 17% probability for an extra Cooper pair to leak via inelastic tunnelling events shown in Fig. 9, during a cycle.

From the preceding experimental results one can conclude that the current transferred by the gate variations, $-2ef\,Q_P$, in the in-phase gate cycles with $f<f_{LZ}$ follows the relation $\Delta I=2ef$ in data measured with amplitudes crossing only one triangle on the gate plane. Here $\Delta I=|I-I_0|$ is the absolute value of the total current with the static leakage current subtracted. However, this suggests that quasiparticle tunnelling plays a minor role when operating in this regime. This is contradicting the general assumption that quasiparticles are tunnelling completely stochastically in both time and direction, which was one of the explanations for the four honeycombs on the DC-modulation plane in Section 4.3. This assumption of all stochastic behaviour should prevent the correct oper-

ation of our in-phase measurement as long as quasiparticle tunnelling is happening at the rate faster than the inverse measuring time $\tau_m^{-1} \leq (100\,\mu s)^{-1}$, which indeed was assumed to explain the result of the DC-modulation measurement.

If the quasiparticle tunnelling is happening less frequently than the frequency of the applied gate signals f, a major reduction in current should be observed due to missed cycles. Yet, the whole principle of operation breaks down due to the undefined and constantly varying trajectory, if these tunnelling events are more frequent than f. Hence, neither of these schemes yields $I = -2ef$.

However, the relatively accurate behaviour in the in-phase measurements can be explained using the energy-minimisation model, which is also consistent with the four honeycombs obtained in the DC-modulation measurements, as explained earlier in Section 4.3. As long as the amplitude is small enough that the system stays near one degeneracy node and thus at the largest possible current given by the different choices of quasiparticle configurations, no quasiparticle tunnelling happens and the system is locked to a certain configuration yielding accurate operation. But, as soon as we increase the amplitude too much the quasiparticle configuration starts to change and thus prevents the accurate transfer. However, if the gate trajectory only shortly goes out of the area of the locked configuration, quasiparticle tunnelling can be prevented by the operating frequency f being faster than the time of quasiparticle tunnelling, and thus the configuration remains locked.

Increase in the bias voltage ($V \gtrsim 80\,\mu V$) has the same effect as increasing the amplitude, since the high current areas (edges of the triangles) corresponding to different quasiparticle configurations start to overlap making the choice for the optimum quasiparticle configuration unclear. At the bias voltages higher than the optimum operation point $V \approx 50\,\mu V$ the triangles of the stability diagram spread too much exceeding the amplitude used and the accuracy of the turnstile kind of behaviour is diminished until at $V \gtrsim 80\,\mu V$ it breaks down. The effect of this can be seen in the I–V curves shown in Fig. 11, which also show that some frequency dependence is still retained after the resonance point $V \gtrsim 80\,\mu V$, but we have no clear model to explain this behaviour due to the existence of many overlapping hysteretic areas corresponding to different quasiparticle configurations.

We also performed measurements using two times larger amplitude ($\sim 1/3 \times 2e$-period) of the in-phase RF signal. The results obtained at $V \simeq -50\,\mu V$ are shown in the last two lines of Table I and plotted in Fig. 13 with a fit by Eq. (6). In the absence of quasiparticle tunnelling and thus with a stable $2e$-periodic stability diagram, one would expect a twice larger

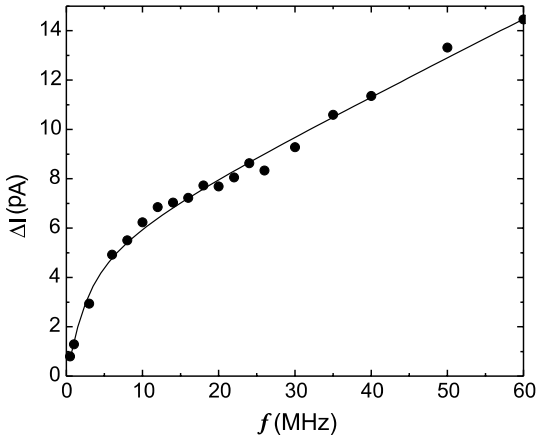

Fig. 13. Current, $\Delta I = |I - I_0|$, at the degeneracy node as a function of the frequency of the applied in-phase RF signal of $\sim 1/3 \times 2e$-period amplitude. The circles correspond to data taken at the optimum bias voltage $V \approx -50\,\mu$V and the solid line is the fit by Eq. (6) with parameters shown on the last row of Table I.

Q_P ($Q_P = 2$) than in the data presented, *e.g.*, in Fig. 12, since the trajectory of gates crosses two triangles during one cycle. This trajectory is shown by the thick dashed arrow and the corresponding $2e$-periodic stability diagram by solid lines in Fig. 14.

As expected, the measurements did not yield such a slope, but about $Q_P \approx 4$ instead, which can be explained with the energy-minimisation model. As seen in Fig. 14, we already move over to the neighbouring triangle corresponding to a different quasiparticle configuration. Thus the configuration is changed from (0,0) to (1,1) and back during every cycle. These two extra quasiparticles responsible for changing the configuration are naturally always driven in the direction of the bias voltage thus yielding extra charge of $2e$ carried during every cycle. If we take into account these two quasiparticles transferred during the cycle and the three triangles we cross, one corresponding to quasiparticle configuration (1,1) and two to (0,0), as shown in Fig. 14, we obtain $8e$ for the total charge carried per cycle. This explains the peculiar result of effectively four Cooper pairs transferred per cycle.

Measurement yields $f_{LZ} \sim 4$ MHz, which is lower than the one, $f_{LZ} \sim 14$ MHz, estimated with the smallest Josephson coupling of $E_J \approx 17\,\mu$eV, obtained from the small amplitude measurements. This deviation is most likely due to the quasiparticle tunnelling involved in the cycle. With our sample parameters the error in quasiparticle transport is already significant at frequencies of few MHz due to the cotunnelling of quasi-

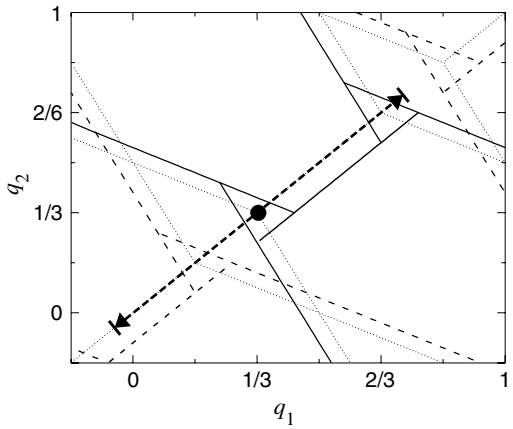

Fig. 14. Trajectory of gates, shown by the thick dashed arrow, in the in-phase measurement using the largest amplitude $\sim 1/3 \times 2e$-period. Thin dotted lines show two honeycomb patterns at $V = 0$ corresponding to quasiparticle configurations $(0, 0)$ and $(1, 1)$. Black circle is the operating point tuned by DC gate voltages. Solid and dashed lines show the $2e$-periodic stability diagrams at $V = 50\,\mu$V corresponding to quasiparticle configurations $(0, 0)$ and $(1, 1)$—respectively.

particles.[12–15] This causes a deviation from the optimum current already at those frequencies and together with the LZ limit of Cooper pair transfer (~ 14 MHz) it yields a smoother double transition starting from $\lesssim 5$ MHz. However, due to the complexity of the energy diagram (see, *e.g.*, Fig. 8) along the path used in the measurement (see Fig. 14) and involution of stochastic quasiparticle tunnelling in the total transfer cycle, we cannot be absolutely certain this is the only explanation. The dynamic leakage current is much higher compared to the data taken with smaller amplitude and interestingly has the dependence of $Q_L \approx 0.5$ which might correspond to a leak of one quasiparticle during the cycle, but may as well be accidental and can also be explained by 50% probability of leakage of a Cooper pair during a cycle.

6. PUMPING MEASUREMENTS

To complement the turnstile-type of in-phase measurements described in Section 5, we also measured the same sample with 90° phase-shifted RF signals applied to the two gates. This provided a circular path around the chosen degeneracy node. The node was again found as described earlier. At non-zero bias voltage one should traverse around the whole triangle to achieve proper pumping. Thus, non-zero bias voltage should allow pump-

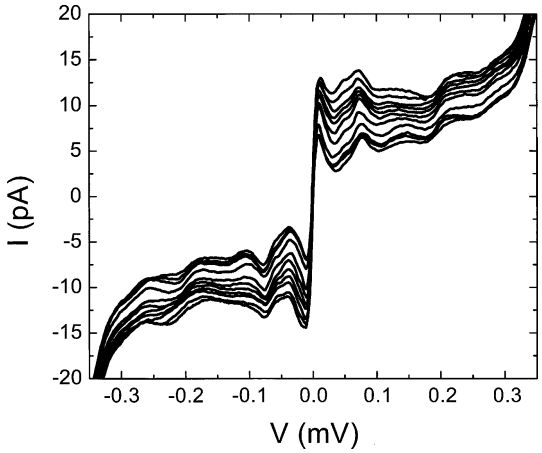

Fig. 15. *I–V* curves measured at one of the degeneracy nodes with sinusoidal RF signal added to the two gates with 90° phase difference. The amplitude of the RF signal was $1/3 \times 2e$-period and the frequencies were 0.1, 0.5, 1, 3, 6, 8, 10, 12, 14, 18, and 22 MHz from the smallest to the highest absolute level of current.

ing as long as neighbouring triangles do not overlap. However, these measurements did not yield as clear results as the in-phase measurements.

We measured the pumped current at several different nodes and with different amplitudes of the RF signal: 1/9, 1/6, 1/4 and 1/3 times the $2e$-period. In Fig. 15 some of the *I–V* curves measured using the largest of these amplitudes are shown. They exhibit clear frequency dependence which, in turn, varies with the bias voltage. The most surprising detail in these *I–V* curves is that they reproduce the turnstile kind of behavior, so that the pumped current is always in the direction of the bias voltage. Thus out-of-phase RF signals increase the bias driven current no matter what direction we wind around the node.

To analyse the 'pumped' current in more detail we examined the current at fixed voltages against frequency. Some examples of these plots are shown in Fig. 16. The general behaviour of the current as a function of the frequency of the out-of-phase RF signals is similar to that observed in the in-phase measurements. The current increases first approximately linearly but the slope decreases at around 30 MHz, which is again most likely due to LZ tunnelling. After that the behaviour has no general tendency. Curves corresponding to different amplitudes or even to same amplitude but different bias voltages differ a lot from each other. The only common feature is that the slope tends to increase again. That is why the fitting of the formula similar to Eq. (6) does not give a satisfactory result.

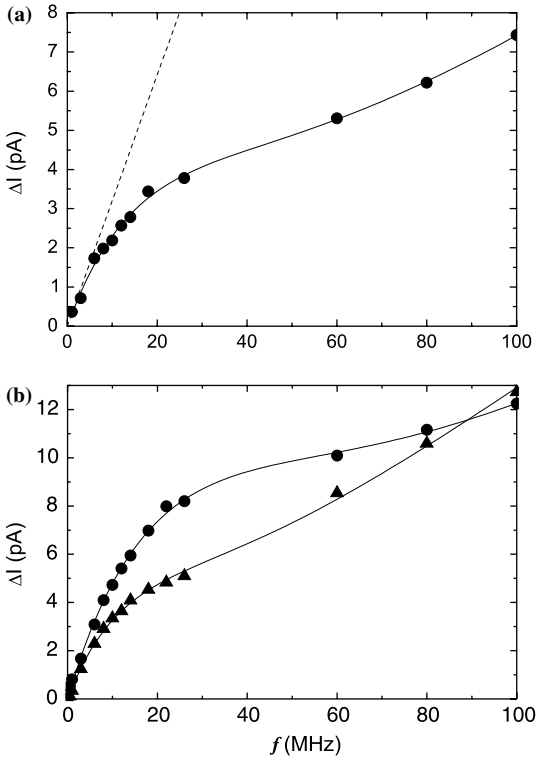

Fig. 16. Current, $\Delta I = |I - I_0|$, as a function of the pumping frequency. The radius of the circular trajectory of gates is $1/4 \times 2e$-period in (a) and $1/3 \times 2e$-period in (b). The data in (a) have been taken at $V \approx 365\ \mu$V and the dashed line corresponds to $\Delta I = 2ef$. Circles and triangles in (b) have been taken at $V \approx 35\,\mu$V ($< 80\mu$V) and $V \approx 305\,\mu$V ($> 80\,\mu$V) yielding the initial slope of $\sim 4e$ and $\sim 3e$, respectively. Solid lines are fits by Eq. (7), with parameters given in Table II.

To find the initial slope and an approximate value of the critical frequency $f_0 \sim f_{LZ}$ for LZ-crossover, we used an empirical function

$$I(f) \equiv -2ef\,Q_P + 2eQ_2\,[1 - exp\,(-f/f_0)]\,f + I_0, \tag{7}$$

which represents an exponential crossover from the initial slope $-2eQ_P$ to another, $-2e(Q_P - Q_2)$, with the transit frequency f_0. The fitting of this function gives more freedom at higher frequencies while it still reproduces the initial slope and f_0 with good accuracy. Here I_0 is again the same static leakage current as in the in-phase measurements. Fig. 16 also shows the function $I(f)$ fitted to the experimental data. The obtained slopes and critical frequencies from the fits using Eq. (7) are shown in Table II.

TABLE II

Results of the data fits of the out-of-phase measurements. Parameters as in Eq. (7)

Ampl. (2e)	V (μV)	Q_P(2e)	f_0 (MHz)
1/9	−83	0.65 ± 0.12	48 ± 16
1/9	83	0.99 ± 0.20	31.5 ± 7.0
1/5	−83	0.97 ± 0.18	26.4 ± 4.6
1/5	83	0.97 ± 0.34	26.2 ± 9.0
1/4	$250 \rightarrow 350$	1.00 ± 0.26	24.0 ± 7.0
1/4	$-350 \rightarrow -70$	0.886 ± 0.060	29.0 ± 2.4
1/4	365	1.000 ± 0.074	22.1 ± 1.6
1/4	−320	0.934 ± 0.086	23.1 ± 2.3
1/4	310	1.05 ± 0.15	22.9 ± 3.4
1/3	75	1.91 ± 0.10	25.1 ± 1.7
1/3	55	1.986 ± 0.062	28.2 ± 1.2
1/3	35	2.130 ± 0.060	32.4 ± 1.4
1/3	−75	1.529 ± 0.094	24.1 ± 1.9
1/3	305	1.53 ± 0.10	16.6 ± 1.1

The resonance point at $V \sim 80\,\mu$V, clearly visible also in Fig. 15 is important in the analysis of these data as it was in the case of in-phase measurements. At the two smallest amplitudes, 1/9 and 1/5 times $2e$-period, frequency dependence of current was seen only at the resonance points. The slope obtained at this voltage is quite close to $2e$ ($Q_P \approx 1$) with both amplitudes. At the amplitude of $1/4 \times 2e$-period the plateau in current was spread over the whole bias range all the way up to the first JQP peak. At bias voltages smaller than the one corresponding to the resonance point the supercurrent masked the frequency dependence. Supercurrent is very sensitive to the setting of gate voltages, and therefore current in this regime is susceptible to even small changes in the trajectory of gates. At the bias voltages higher than the resonance point, systematic and rather stable frequency dependence was restored yielding the slope of $Q_P \approx 1$. Data fits at this RF amplitude and bias voltage of $V \approx 365\,\mu$V are shown in Fig. 16(a). The dashed line shows $\Delta I = 2ef$. At the highest amplitude, $1/3 \times 2e$-period, the frequency dependence of current is very distinctive as seen in the I–V curves in Fig. 15. The obtained frequency dependencies split into two categories again. At bias voltages smaller than the resonance one $V \approx 80\,\mu$V the initial slope is approximately $Q_P \approx 2$ while at voltages higher than the resonance one this slope is smaller with average at around $Q_P \approx 1.5$. Examples of both of these cases are shown in

Fig. 16(b). The obtained critical frequency, f_0, is always of the same order ~ 30 MHz as in the in-phase measurements, thus further suggesting it to originate from LZ events.

It is noteworthy that out-of-phase gate control does not make a distinction whether the phase difference is $+90^\circ$ or -90°. This is the second feature besides the bias dependence indicating that we do not pump charges in the traditional sense. Direction of the obtained current is determined only by the bias voltage whereas the pumping frequency and radius determine the magnitude. This can be explained in approximately the same way as the in-phase measurement, where the system always chose the lowest energy state when passing a resonance. When trying to pump against the bias voltage the resonance point for cotunnelling to happen is reached before the resonance of single tunnelling as can be seen in Fig. 2. It is likely that in our experiment cotunnelling is so strong that, it always happens first. This cycle of cotunnelling yields a transfer of two Cooper pairs during one cycle, which is twice as much as in pumping in the direction of bias.[31] However, this was not the case in our measurements which yielded $\Delta I \approx 2ef$ in both directions. This discrepancy could be due to $\sim 33\%$ suppression of cotunnelling, which sounds reasonable as we can estimate f_{LZ} for cotunnelling in case of, *e.g.*, the amplitude of $1/4 \times 2e$-period, to be of the order of few MHz, which would suggest rather high suppression.

One possible explanation for the discovered behaviour arises from the circular pumping trajectory. Due to the structure of the stability diagram, $E_{\mathrm{J}}^{\mathrm{co}}$ between the states $|10\rangle$ and $|01\rangle$ along the circular path is suppressed by the factor $\sqrt{5/2}$ more as compared to other cotunnelling events along the trajectory. This directly leads to the reduction of f_{LZ} to $2/5 \times f_{\mathrm{LZ}}$ and thus to almost doubling of P_{LZ} in the middle junction at $f \approx f_{\mathrm{LZ}} \sim 2$ MHz. This again could prevent the cotunnelling in the middle junction (but not in the other two) and thus yield a $\sim 33\%$ suppression of the total cotunnelling probability, which would prevent a cycle transferring one Cooper pair against the bias voltage as in the experiments.

7. DISCUSSION

To further discuss the validity of the energy-minimisation model and the model developed for the turnstile-kind of behaviour, we briefly review some of the earlier measurements of the CPP or similar devices. Somewhat similar turnstile-kind of behaviour in the case of a superconducting SET has been reported earlier in Ref. 33. The principle of operation in that particular experiment was based on a similar asymmetric behaviour of the system when passing a resonance point.[57] The main difference besides the number of junctions (two in that case), was that in that

experiment Cr resistors were embedded near the sample to provide the required dissipation. These resistors also suppressed any current near the zero voltage and thus the current plateaus were only seen at a finite voltage between $E_C/2e$ and $2\Delta/e$. (Our measurement indicates that no additional resistances are necessary to obtain this behaviour.) Relatively accurate result of the experiment is consistent with the energy-minimisation model, since the gate trajectory they used in Ref. 33 stayed all the time close to a resonance point and thus close to the peak in supercurrent. However, this peak in supercurrent was suppressed due to the resistive environment, which might have increased the probability of quasiparticle tunnelling, yielding a reduced accuracy in 'pumping': This agrees with the experiment as they reported current which was inferior to $I=-2ef$ at the plateaus observed.

Our out-of-phase measurement along the circular path around the degeneracy node also yielded current $-2ef$ but the direction was defined only by the bias voltage as in the in-phase measurements. The proper direction of current, depending on the direction of pumping and not on the bias voltage, was observed in the measurements of the CPP by Geerligs *et al.*[31] This difference is most probably due to the smaller ratio $E_J/E_C \approx 0.03$ in that experiment, which reduced the probability of cotunnelling significantly. This suppression is also consistent with a lower LZ frequency, f_{LZ}, obtained in that experiment and the lack of the zero bias supercurrent, which prevented the measurement of the DC modulation. Yet, a small step in a pumped current at $V=0$ remained as a consequence of cotunnelling, but the small height of it indicates much higher suppression of cotunnelling than in our experiment. Geerligs *et al.* also state that the step was significantly larger in another sample, even reversing the current, which is what we observe.

The pumping trajectory used in Ref. 31 was very wide and according to the energy-minimisation model the quasiparticle configuration should have changed several times during each cycle. On the contrary the measurement yielded rather accurate behaviour, which would indicate no change of the quasiparticle configuration during the operation. This could be explained by the fact that quasiparticles had no freedom to tunnel and a certain configuration remained locked all the time, thus resulting in pure $2e$-periodic stability diagram, which is also reported, *e.g.*, in Ref. 58. The failure of measuring the DC modulation in the superconducting state in Ref. 31 can be explained by the lack of supercurrent (small E_J), since there should not be current flowing inside the opened triangles of the stability diagram at $V \neq 0$, which was used to map the degeneracy nodes in the normal state. This can be verified by the measurement of Fig. 7(b).

As mentioned in the previous paragraph the pure $2e$-periodic stability diagram without any quasiparticle poisoning has been observed in the device with three junctions in series.[58] The result was achieved by fabricating the middle junction much more transparent than the outer ones, thus making the device more like the superconducting SET (SSET) in which the $2e$-periodicity has been observed in many experiments. Another trick could be to modify the superconducting gap of the islands to be larger than those of the electrodes as in Ref. 59, where the method was observed to reproducible deliver pure $2e$-periodicity in the case of SSET. Obtaining pure $2e$-periodicity would allow more precise operation of the device without the limitations set by the energy-minimisation model. Furthermore, the idea of larger gap of the islands could be realised by fabricating them out of different superconducting material, *e.g.*, niobium.

In the measurement of Ref. 19 a similar idea of resistive environment as in Ref. 33 was used, now in the case of a CPP. The influence of the resistive environment was to suppress the otherwise strong cotunnelling of Cooper pairs. The experimental results showed suppression of current near the zero bias as in Ref. 33 and thus the current plateaus were again obtained only at higher bias voltages. These plateaus were very weak and yielded a behaviour similar to our measurement. The value of the pumped current was approximately $-2ef$ but the direction was determined just by the bias voltage. This could be due to inability of the Cr resistors to prevent the cotunnelling in spite of the small ratio $E_J/E_C \approx 0.013$. As stated in Ref. 19 the quasiparticles were actively present also in that experiment.

8. CONCLUSIONS

We have shown that current in both the in-phase and out-of-phase gate cycles follows the relation $\Delta I = 2ef$ in data measured with amplitudes crossing or encircling only one triangle on the gate plane. These experiments also demonstrate in practise how CPP could be used as a turnstile with help of dissipation. A model was developed to explain the process and experiments clearly demonstrated this behaviour quantitatively.

The failure to observe pure $2e$-periodicity in the DC-modulation measurement indicates an active presence of non-equilibrium quasiparticles in the system, as in many earlier experiments.[19,31,60,61] However, the agreement between the model developed for the turnstile-kind of behaviour and the measurements suggests that quasiparticle tunnelling has a minor effect when operating in this regime, which is contradicting the general assumption that quasiparticles are tunnelling completely stochastically. To

explain this twofold behaviour of the system, a model was developed, which is based on a very general tendency of a system to always strive for minimum energy. It suggests that if the quasiparticles in the system have freedom to move, they will organize themselves to the configuration yielding the highest current, which continuously lowers the energy of the system. The four honeycombs obtained in the DC-modulation measurement are consistent with this model and the relatively accurate behaviour in the RF-measurements can be explained with it, too. The model also agrees with the earlier measurements of the CPP[19,31] and another similar device.[33]

We also measured the current pumped through the array by winding around a degeneracy node along a circular path. This showed the correct magnitude in obtained current but the direction was not defined by the direction of pumping but it was rather determined by the bias voltage thus reproducing the turnstile kind of behaviour. This behaviour could be explained in general terms, although not as precisely as in the case of in-phase measurements, by the similar energy minimisation argument, that the system chooses the state corresponding to a lower energy when the resonance is passed adiabatically. This does not fully explain the observed magnitude of current $\Delta I = 2ef$ when pumping in the direction against the bias voltage. But, it agrees with a strong cotunnelling in our experiment, which is due to the large ratio of $E_J/E_C \approx 0.15$.

As a final note we state that it is unlikely for CPP as such to be able to provide a current standard or otherwise work with high accuracy. The strong cotunnelling and relaxation, among other uncontrollable processes, tend to degrade the pumping cycles. However, there might be ways, such as embedding the sample in a highly resistive environment,[19] or using a combined flux and charge control,[20,62] or preventing the quasiparticle poisoning more efficiently,[58,59] to overcome these difficulties. Moreover, until so far there exists no pumping measurement of the CPP in which the stability diagram would have verifiably shown pure $2e$-periodicity. Thus, it is not yet possible to definitely state how accurately the CPP would operate under perfect conditions. Also the use of the CPP to measure, *e.g.*, decoherence time would need much more controlled electromagnetic environment to be successful.[27,28]

ACKNOWLEDGMENTS

The authors wish to thank A. Halvari for fabrication of the sample and K. Hansen and M. Aunola for fruitful discussions and comments. This work has been supported by the Academy of Finland under the Finnish Centre of Excellence Programme 2000–2005 (Project No. 44875,

Nuclear and Condensed Matter Programme at JYFL) and partially supported by EU (Project SQUBIT2), National Graduate School in Materials Physics, and Finnish Academy of Science and Letters (Väisälä rahasto).

REFERENCES

1. D. J. Thouless, *Phys. Rev. B* **27**, 6083 (1983).
2. L. P. Kouwenhoven, A. T. Johnson, N. C. van der Vaart, C. J. P. M. Harmans and C. T. Foxon, *Phys. Rev. Lett.* **67**, 1626 (1991).
3. J. M. Shilton, V. I. Talyanskii, M. Pepper, D. A. Ritchie, J. E. F. Frost, C. J. B. Ford, C. G. Smith and G. A. C. Jones, *J. Phys. Cond. Matter* **8**, L531 (1996).
4. V. I. Talyanskii, J. M. Shilton, M. Pepper, C. G. Smith, C. J. B. Ford, E. H. Linfield, D. A. Ritchie and G. A. C. Jones, *Phys. Rev. B* **56**, 15180 (1997).
5. H. Pothier, P. Lafarge, P. F. Orfila, C. Urbina, D. Esteve and M. H. Devoret, *Physica* B **169** 573 (1991) [*Europhys. Lett.* **17**, 249 (1992)].
6. M. W. Keller, J. M. Martinis, N. N. Zimmerman and A. H. Steinbach *Appl. Phys. Lett.* **69**, 1804 (1996).
7. M. W. Keller, J. M. Martinis and R. L. Kautz, *Phys. Rev. Lett.* **80**, 4530 (1998).
8. K. K. Likharev and A. B. Zorin *J. Low Temp. Phys.* **59**, 347 (1985).
9. D. V. Averin and Yu. V. Nazarov, *Phys. Rev. Lett.* **65**, 2446 (1990).
10. D. V. Averin and A. A. Odintsov, *Phys. Lett. A* **140**, 251 (1989).
11. L. J. Geerligs, D. V. Averin and J. E. Mooij, *Phys. Rev. Lett.* **65**, 3037 (1990).
12. H. D. Jensen and J. M. Martinis, *Phys. Rev. B* **46**, 13407 (1992).
13. D. V. Averin, A. A. Odintsov and S. V. Vyshenskii, *J. Appl. Phys.* **73**, 1297 (1993).
14. J. M. Martinis, M. Nahum and H. D. Jensen, *Phys. Rev. Lett.* **72**, 904 (1994).
15. L. R. C. Fonseca, A. N. Korotkov and K. K. Likharev, *Appl. Phys. Lett.* **69**, 1858 (1996).
16. J. M. Ziman, *Principles of the Theory of Solids* (Cambridge University Press, Cambridge, UK, 1964).
17. J. P. Pekola, J. J. Toppari, M. Aunola, M. T. Savolainen and D. V. Averin, *Phys. Rev. B* **60**, R9931 (1999).
18. M. Aunola, J. J. Toppari and J. P. Pekola, *Phys. Rev. B* **62**, 1296 (2000).
19. A. B. Zorin, S. A. Bogoslovsky, S. V. Lotkhov and J. Niemeyer, in *Macroscopic Quantum Coherence and Quantum Computing*, edited by D. V. Averin, B. Ruggiero, and P. Silverstrini, MQC^2 Instituto Italiano per gli Studi Filosofici (Kluwer Academic / Plenum, New York, 2001), p. 147
20. A. O. Niskanen, J. P. Pekola, and H. Seppä, *Phys. Rev. Lett.* **91**, 177003 (2003).
21. Y. Nakamura, Y. A. Pashkin and J. S. Tsai, *Nature* **398**, 786 (1999).
22. J. R. Friedman, V. Patel, W. Chen, S. K. Tolpygo, and J. E. Lukens, *Nature* **406**, 43 (2000).
23. C. H. van der Wal, A. C. J. ter Haar, F. K. Wilhelm, R. N. Schouten, C. J. P. M. Harmans, and J. E. Mooij, *Science* **290**, 773 (2000).
24. D. Vion, A. Aassime, A. Cottet, P. Joyez, H. Pothier, C. Urbina, D. Esteve, and M. H. Devoret, *Science* **296**, 886 (2002).
25. Y. Makhlin, G. Schön, and A. Shnirman, *Rev. Mod. Phys.* **73**, 357 (2001).
26. D. V. Averin, *Solid State Commun.* **105**, 659 (1998).
27. J. P. Pekola, and J. J. Toppari, *Phys. Rev. B* **64**, 172509 (2001).
28. R. Fazio, F. W. J. Hekking, and J. P. Pekola, *Phys. Rev. B* **68**, 054510 (2003).
29. K. A. Matveev, M. Gisselfält, L. I. Glazman, M. Jonson, and R. I. Shekhter, *Phys. Rev. Lett.* **70**, 2940 (1993).
30. P. Joyez, P. Lafarge, A. Filipe, D. Esteve, and M. H. Devoret, *Phys. Rev. Lett.* **72**, 2458 (1994).

31. L. J. Geerligs, S. M. Verbrugh, P. Hadley, J. E. Mooij, H. Pothier, P. Lafarge, C. Urbina, D. Esteve, and M. H. Devoret, *Z. Phys. B* **85**, 349 (1991).
32. M. Aunola, *Phys. Rev. B* **63**, 132508 (2001).
33. S. V. Lotkhov, S. A. Bogoslovsky, A. B. Zorin, and J. Niemeyer, in *International Workshop on Superconducting Nano-Electronics Devices*, edited by J. P. Pekola, B. Ruggiero, and P. Silvestrini, SNED (Plenum, Naples, Italy, 2001), p. 105.
34. D. V. Averin, and K. K. Likharev, in *Mesoscopic Phenomena in Solids*, edited by B. L. Althschuler, P. A. Lee, and R. A. Webb (North-Holland, Amsterdam, 1991), p. 213.
35. A. M. van den Brink, A. A. Odintsov, P. A. Bobbert, and G. Schön, *Z. Phys. B* **85**, 459(1991).
36. E. N. Bibow, Ph.D. thesis, de l'Université Joseph Fourier—Grenoble I en Physique (2001).
37. M. V. Berry, *Proc. R. Soc. London, Ser. A* **392**, 45 (1984).
38. M. Aunola and J. J. Toppari, *Phys. Rev. B* **68**, 20502 (2003).
39. P. Lafarge, P. Joyez, D. Esteve, C. Urbina and M. H. Devoret, *Nature* **365**, 422 (1993).
40. A. B. Zorin *Rev. Sci. Instrum* **66**, 4296 (1995).
41. D. Vion, P. F. Orfila, P. Joyez, D. Esteve and M. H. Devoret *J. Appl. Phys*. **77**, 2519 (1995).
42. The circuit has been designed and contructed by Kari Loberg and controlling software has been done using Lab View® by Sampo Tuukkanen at the Department of Physics, University of Jyväskylä.
43. T. A. Fulton P. L. Gammel, D. J. Bishop, L. N. Dunkleberger, and G. J. Dolan, *Phys. Rev. Lett* **63**, 1307 (1989).
44. D. V. Averin and V. Ya. Aleshkin *Pis'ma Zh. Éksp. Teor. Fiz*. **50**, 331 (1989) [*JETP Lett*. **50,** 367 (1989)]
45. Y. Nakamura, C. D. Chen and J. S. Tsai *Phys. Rev. B* **53**, 8234 (1996).
46. V. Ambegaokar and A. Baratoff *Phys. Rev. Lett*. **10**, 486 (1963), Erratum **11**, (1963) 104.
47. M. Tinkham *Introduction to Superconductivity* 2nd *ed*. (McGraw-Hill, New York, 1996), pp. 257–277.
48. S. Farhangfar, K. P. Hirvi, J. P. Kauppinen, J. P. Pekola, J. J. Toppari, D. V. Averin, and A. N. Korotkov *J. Low Temp. Phys*. **108**, 191 (1997).
49. M. T. Tuominen, J. M. Hergenrother, T. S. Tighe and M. Tinkham *Phys. Rev. Lett*. **69**, 1997 (1992).
50. G.-L. Ingold and Yu. V. Nazarov, *Single Charge Tunnelling, Coulomb Blockade Phenomena in Nanostructures*, edited by H. Grabert and M. H. Devoret (Plenum, New York, 1992), ch. 2, p. 21.
51. M. Tinkham, J. M. Hergenrother, and J. G. Lu, *Phys. Rev. B* **51**, 12649 (1995).
52. R. C. Dynes and J. P. Garno, *Phys. Rev. Lett*. **53,** 2437 (1984).
53. J. P. Pekola, T. T. Heikkilä, A. M. Savin, J. T. Flyktman, F. Giazotto, and F. W. J. Hekking, *Phys. Rev. Lett.* **92**, 056804 (2004).
54. K. Andersson, P. Delsing, and D. Haviland, *Phys. B* **248–288**, 1816 (2000).
55. L. J. Geerligs, V. F. Anderegg, P. A. M. Holweg, J. E. Mooij, H. Pothier, D. Esteve, C. Urbina, and M. H. Devoret, *Phys. Rev. Lett*. **64**, 2691 (1990).
56. J. Delahaye, J. Hassel, R. Lindell, M. Sillanpää, M. Paalanen, H. Seppä and P. Hakonen, *Science* **299**, 1045 (2003).
57. P. Ao and J. Rammer, *Phys. Rev. B* **43**, 5397 (1991).
58. E. Bibow, P. Lafarge, and L. P. Lévy, *Phys. Rev. Lett*. **88**, 017003 (2002).
59. J. Aumentado, M. W. Keller, and J. M. Martinis, *Phys. Rev. Lett*. **92**, 066802 (2004).
60. L. J. Geerligs, V. F. Anderegg, J. Romijn, and J. E. Mooij, *Phys. Rev. Lett*. **65**, 377 (1991).
61. P. Lafarge, H. Pothier, E. R. Williams, D. Esteve, C. Urbina, and M. H. Devoret, *Z. Phys. B*, **85**, 327 (1991).
62. A. Romito, F. Plastina, and R. Fazio (2002), cond-mat/0212414.